Mineral Petrol (2008) 92: 427–452
DOI 10.1007/s00710-007-0213-5
Printed in The Netherlands

Mineralogy and Petrology

Character and significance of spectacular layering features developed in the thin, alkali-basaltic sills of the Ulvö Gabbro Complex, Sweden

S. Å. Larson[1], **K. J. Hogmalm**[1], **W. P. Meurer**[1,2]

[1] Earth Sciences Centre, Department of Geology, Göteborg University, Göteborg, Sweden
[2] Department of Geosciences, University of Houston, Houston, Texas, U.S.A.

Received August 30 2006; Accepted June 29 2007; Published online November 22 2007

Editorial handling: G. Hoinkes

Summary

The Ulvö Gabbro Complex consists of alkali-olivine basaltic circular bodies ~30–80 km in diameter. These intrusions were emplaced at shallow depths (~3 km) as thin sheets (~300 m). Among other things, the gabbroic cumulates of the complex display: modal layering, grain-size variations, trough structures, and slump structures. The crystallization sequence is olivine + plagioclase, ulvöspinel, clinopyroxene, and apatite. A nearly continuous exposure across one of these intrusions, the Norra Ulvön gabbro, is subdivided into: a Lower Zone (LZ), a Rhythmically Layered Zone (RZ) and an Upper Zone (UZ). LZ and RZ were formed at the floor, while UZ grew from the roof downward. Major-element variations in the cores of the cumulus minerals define fractionation trends from the base of the intrusion to the RZ-UZ boundary interpreted as a ''sandwich horizon''. Modeling suggests that a significant amount of crystallized interstitial liquid is required to produce the observed stratigraphic relations. Our results suggest that the small size and shallow emplacement depth of the intrusions of the Ulvö Gabbro Complex helped to preserve evidence of primary accumulation processes. However, it is also clear that despite the limited time available postcumulus processes such as diffusional homogenization and compaction of some grains were important.

Correspondence: S. Å. Larson, Earth Sciences Centre, Department of Geology, Göteborg University, POB 460, SE 40530 Göteborg, Sweden
e-mail: svenake@gvc.gu.se

Introduction

Studies of physical and chemical processes in layered intrusions are essential components of our understanding of magma chambers processes (e.g. Cawthorn, 1996). This study concerns the Ulvö Gabbro Complex, central Sweden, the type locality of ulvöspinel (Mogensen, 1946). Although $\leq$300 m thick and emplaced at shallow depths, gabbros of the Ulvö Gabbro Complex show spectacular igneous layering features that are comparable to those documented from much larger layered intrusions. The combination of the small size and abundant layering features make the Ulvö Gabbro Complex an ideal place to study magma chamber processes.

Before the cumulus and postcumulus processes in layered intrusions can be understood, adequate descriptions of mineralogical and chemical variations are required. This study is primarily directed at characterizing the Ulvö Gabbro Complex in general and in particular the Norra Ulvön gabbro (NUG) as exposed on the Norra Ulvön island (Fig. 1). We include descriptions and interpretations of the various layering features seen in the Ulvö Gabbro Complex and an estimate of the liquid composition parental to these intrusions. We then focus on the Norra Ulvön gabbro providing a detailed modal and mineral chemical stratigraphy. There the upper and lower gabbro contacts border with the Nordingrå granite (Lundqvist,

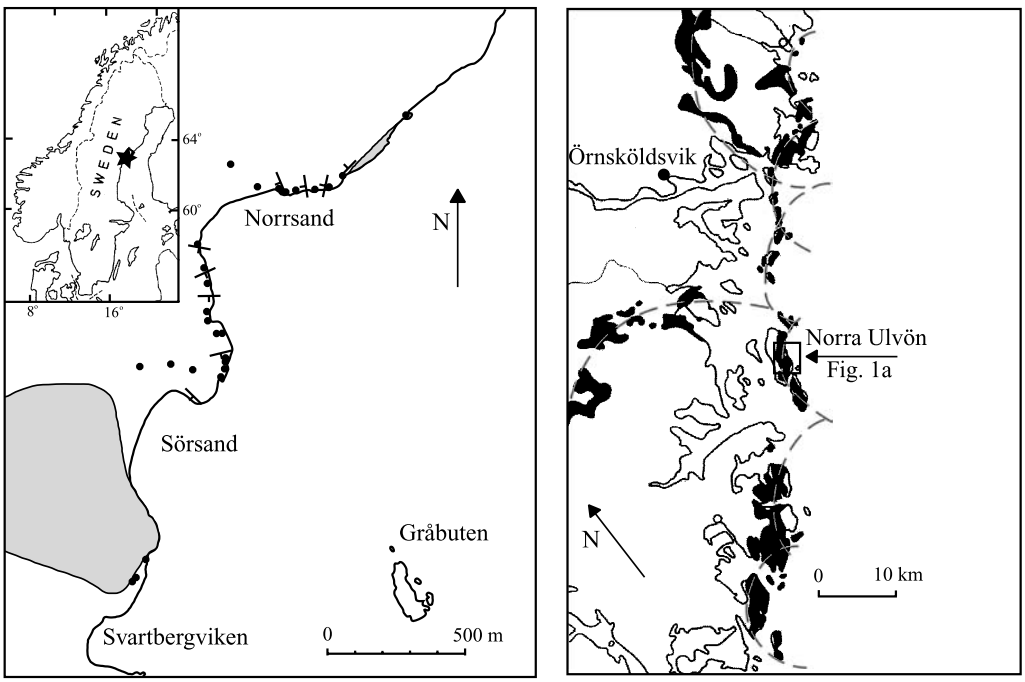

Fig. 1. Right: the Ulvö Gabbro Complex (black) outcropping along the Bothnian Sea shoreline (modified from Lundqvist, 1990). The sheet-like bodies constitute a series of circular bodies of lopolithic shape (outlined by dashed, gray lines). The study area is situated on the island Norra Ulvön. Left: blow up of study site at Norra Ulvön. Sample sites (black dots) and orientation of igneous layering are shown. Gray areas represent granitic host rock representing floor to the north (Norrsand) and roof to the south (Sörsand)

1990) and a gravity survey reveals no significant faults (Larson and Magnusson, 1979).

Geological setting and previous work

The Meso- and Paleo-Proterozoic rocks of the central part of the Baltic Shield host the ~1.25 Ga old (Hogmalm et al., 2006), flat lying gabbroic rocks of the Central Scandinavian Dolerite Group (Welin and Lundqvist, 1975; Gorbatschev et al., 1979; Lundqvist, 1990). Of these, the intrusions that outcrop along the east coast of Sweden (Nordingrå area; Fig. 1) have been named the Ulvö Dolerite Complex (Larson, 1980). They have seen no regional metamorphic overprint and are gently dipping, more or less circular lopoliths ~30 to ~80 km in diameter (Lundqvist, 1990). The thicknesses of the different gabbro sheets are ~250–300 m (Lundqvist and Samuelsson, 1973; Larson and Magnusson, 1979) and estimated intrusion depth of the Norra Ulvön Gabbro is ~2–3 km (Larson and Magnusson, 1976). Feeders are not recognized in the coastal region but may be represented by numerous dolerite dikes traced by magnetic measurements inland (Lundqvist, 1990). Because the intrusions are composed of layered gabbroic rocks they are more properly named ''the Ulvö Gabbro Complex'', a name that will be adopted in the following.

The Ulvö Gabbro Complex has been the subject of petrologic research for the last ~150 years (e.g. Erdmann, 1846, 1848; Dellvik, 1874, 1875; Törnebohm, 1877; Högbom, 1893, 1909a,b; Lundbohm, 1893; Sobral, 1913; Eckerman, 1938, 1946, 1947; Mogensen, 1946). The intrusion has also received more recent attention (Larson, 1973, 1980; Lindh, 1973; Lundqvist and Samuelsson, 1973; Samuelsson, 1973; Larson and Magnusson, 1976, 1979; Magnusson and Larson, 1977; Lundqvist, 1990). Of these Lundbohm (1899), Sobral (1913) and Lundqvist (1990) published maps showing the extension of the Ulvö Gabbro Complex while Mogensen (1946) was the first to describe ulvöspinel naturally present in a rock. The work of Lundqvist and Samuelsson (1973) and Larson (1980) are the only studies directed at documenting the stratigraphic variation in these gabbros.

Field relations in the Ulvö Gabbro Complex

Igneous layering

Although the detailed stratigraphy of gabbro bodies in the Ulvö Gabbro Complex may differ, they all have igneous layering characterized by mafic layers alternating with more felsic layers (Fig. 2a). The layers are commonly rhythmic and usually dip between 10° and 20° (Fig. 1b). Gravity measurements reveal that the dip of the igneous layering is parallel to the intrusive contacts with country rocks (Larson and Magnusson, 1979; Larson, 1980). Whether a layer is considered mafic or felsic is relative and related to the composition of the surrounding layers. Single layers can be traced for >50 m across outcrops. Most layers are ~10 cm thick but may vary from approximately 0.5 cm to 1 m. Individual layers are essentially homogeneous, but some normal and reverse mineral grading occurs (Fig. 2b, c). In some places, grain size differences between mafic and felsic layers are distinct. Centimeter-scale

(a)

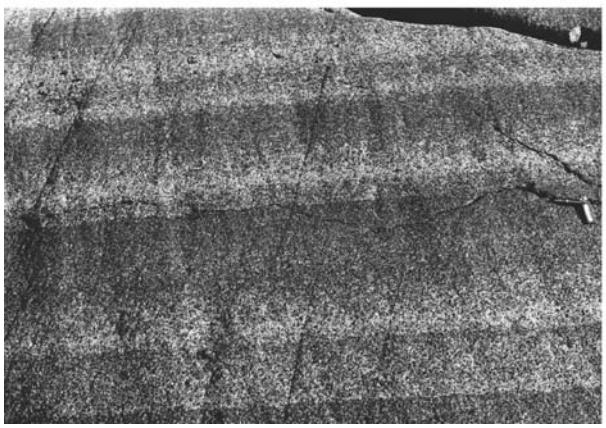

(b)

(c)

Fig. 2. (**a**) Rhythmic layering of alternating dark and light layers showing distinctcontacts (back pack is 60 cm high). (**b**) Reverse graded layering with distinct contacts. (**c**) Detail of normally graded rhythmic layering

layering is also present and can be rhythmically distributed but some are intercalated with layers of the more typical ∼10 cm thickness (Fig. 3a). One example of cm-scale layering is cut by angular unconformities, above which the layering consists of similar cm-scale layers (Fig. 3b).

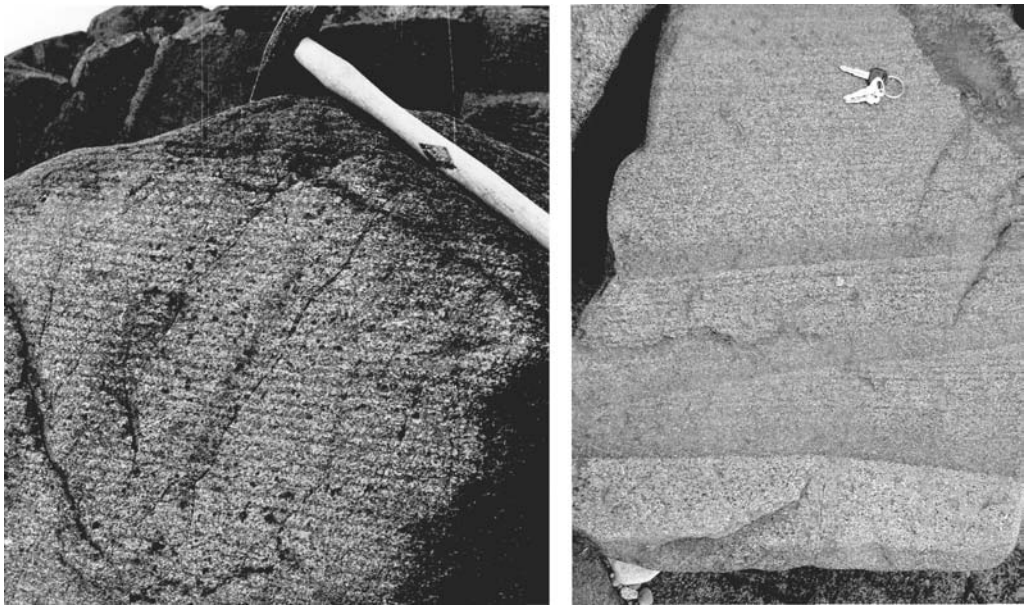

(a) (b)

Fig. 3. (**a**) Small-scale, rhythmic layering (cm-scale). (**b**) Discordant dm size layers in a sequence of small-scale layers

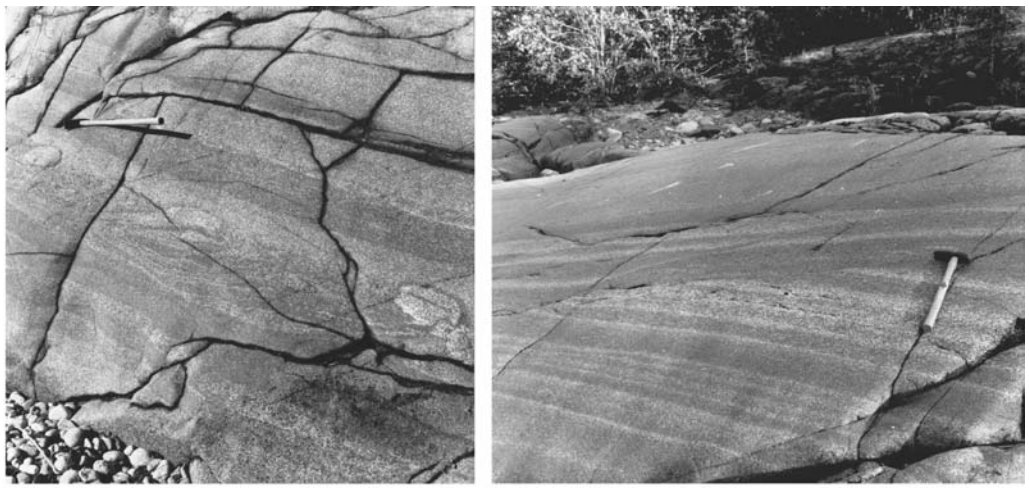

(a) (b)

(c)

Fig. 4. (**a**) Slumping confined to a specific layer. (**b**) Discordance in rhythmic layers. (**c**) Trough structure with concentration of dark minerals to the trough bottom

Disturbed layering

Disrupted and irregular layering features such as slump structures, angular unconformities, and trough structures are relatively common in the rhythmically layered sequences of the Ulvö Gabbro Complex. Small-scale slump structures consist of modally heterogenous horizons in which modally distinct fragments of layers are found (Fig. 4a). Discordant layers are similar in appearance to low-angle unconformities in sedimentary rocks although no evidence of erosion has been documented (Fig. 4b). Trough structures are synformal stacks of layers with heights of 0.1–3 m and widths of 1–20 m and show mafic mineral accumulations at their bottoms (Fig. 4c). Some small troughs are linked to each other by antiformal structures like low amplitude folds. The trough axes tend to be approximately perpendicular to the strike of the general layering and undisturbed layers are found both above and below the troughs.

Foliation

An igneous foliation (locally a lineation), defined by aligned plagioclase, is common in the layered portions of the Ulvö Gabbro Complex. It is most easily recog-

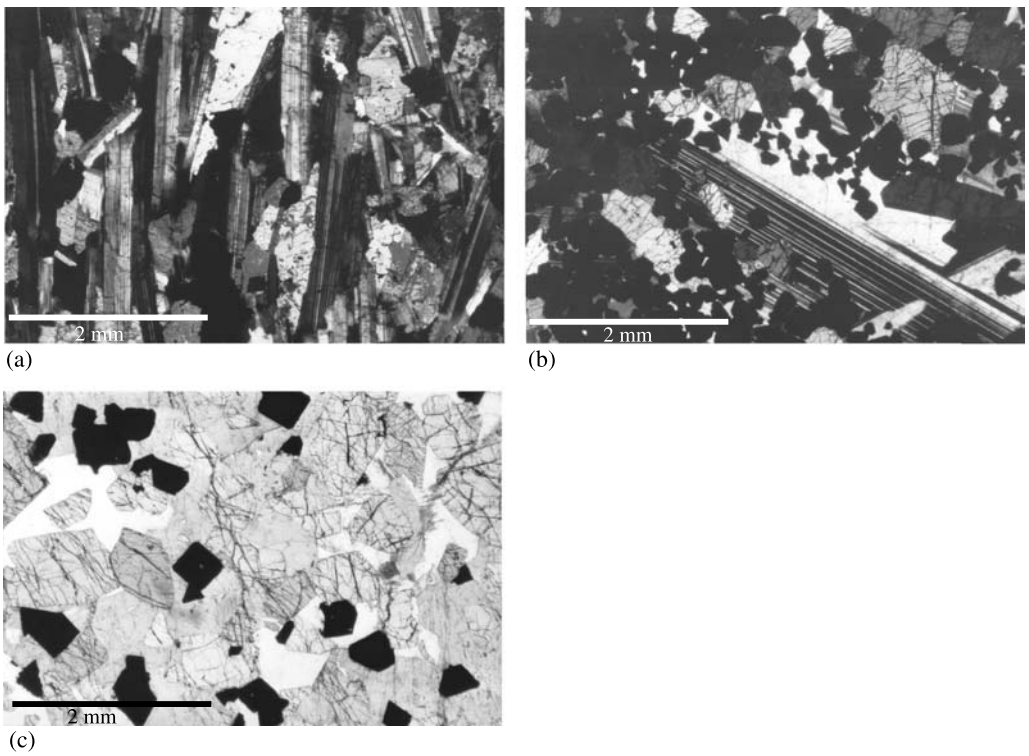

Fig. 5. (**a**) Plagioclase lamination in a light layer from RZb. Length of photograph = 5 mm. (**b**) Dark layer in RZa showing plagioclase core with a postcumulus rim with entrapped cumulus crystals of Fe-Ti oxide (black) and olivine (gray and fractured) crystals. Note the small grain size and euhedral shape of the entrapped Fe-Ti oxide. Length of photograph = 5 mm. (**c**) Dark layer in RZa characterised by euhedral cumulus olivine (gray and fractured), cumulus Fe-Ti oxide (black), and interstitial clinopyroxene (light gray) and plagioclase (white). Length of photograph = 5 mm

nized in plagioclase-rich layers and is most distinct in the RZ of the NUG (Fig. 5a). In many mafic layers there is insufficient plagioclase to define a foliation and the plagioclase present is poikilitic due to postcumulus overgrowths (Fig. 5b and c).

Plagioclase-rich segregations and clots

Plagioclase-rich segregations are common throughout the Ulvö Gabbro Complex. In the Norra Ulvön gabbro they are a few centimeters thick and up to 2–3 m long with lower mafic margins locally developed in the LZ. They have the appearance of thin, laterally discontinuous, disrupted felsic layers (Fig. 6a). Plagioclase-

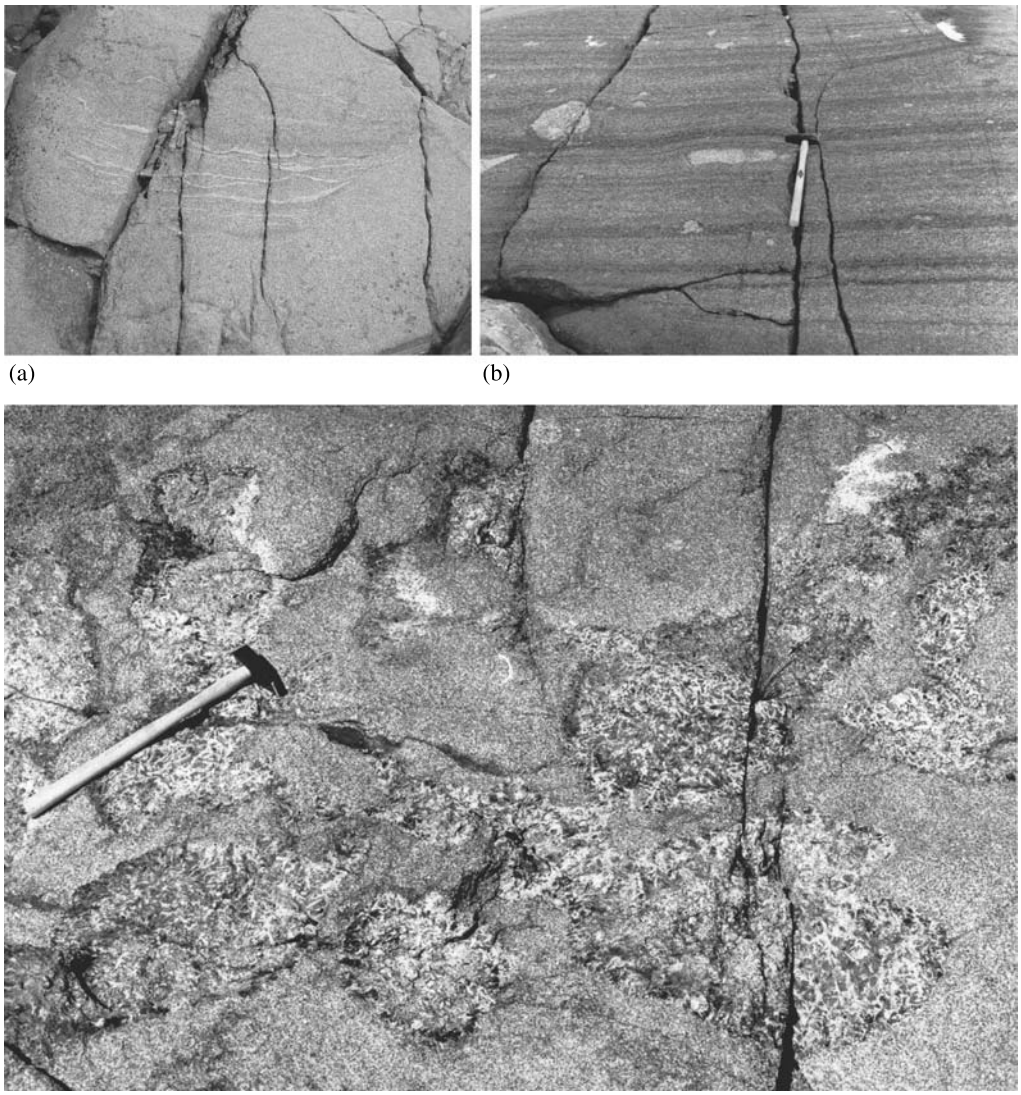

Fig. 6. (**a**) Plagioclase schlieren with fringes of mafic minerals. Note the wavy appearance of layers. (**b**) Plagioclase rich clots and lenses distributed in fragmental layers. Note bending of layers above fragments. (Hammer is 40 cm long). (**c**) Gabbro pegmatitoid clots

rich clots are found in the RZ that are sub-rounded, flattened or irregular with most less than 50 cm in maximum dimension. These are sometimes spatially associated with gabbroic pegmatoids. The layers above are draped over the clots while those beneath are mostly undisturbed. Locally, clots are restricted to specific layers forming ''fragmental layers'' (Fig. 6b).

Gabbroic pegmatoid

Gabbroic pegmatoids occur as small-scale dikes and segregation pods of extremely coarse-grained gabbro (Fig. 6c) and as larger stratiform bodies typically a few 10s of cm thick. Smaller gabbroic pegmatoids are common in areas characterized by slumping and disturbed layering and also related to the plagioclase-rich clots. Although present throughout, pegmatoids are more common in the layered and upper parts of the gabbros.

Petrography

The most abundant minerals are plagioclase, olivine, clinopyroxene, and Fe-Ti oxides. Common accessory minerals include biotite, apatite and ilmenite. The NUG is divided into three zones: the Lower Zone (LZ), the Rhythmically Layered Zone (RZ), and the Upper Zone (UZ; Larson, 1980). The LZ has more olivine than clinopyroxene, and a relatively low modal content of Fe-Ti oxides although exceptions are found. Rhythmic layering in the LZ is rare and usually consists of a few cm thick layers separated by thick sequences of more uniform gabbro. The RZ is subdivided into two sub-zones; RZa has cumulus olivine and interstitial clinopyroxene and abundant cumulus Fe-Ti oxides, while RZb has cumulus clinopyroxene, less than 5% modal olivine, and a well-developed plagioclase foliation. The UZ has more clinopyroxene than olivine and no plagioclase foliation. Fe-Ti oxides are most abundant in the RZ with concentrations of $>50\%$ in a $\sim$10 cm thick mafic layer in RZa. These Fe-Ti oxide rich layers were mined for V at other places in the Ulvö Gabbro Complex. Accessory biotite is irregularly distributed (modal abundance $\sim$1–5%). Apatite mode is limited to 1.5% but since it is essentially impossible to estimate its mode in hand-sample it could be higher in other samples.

The grain-size increases from the margins inward. A 5 cm wide chilled margin consisting of plagioclase-olivine-phyric (phenocrysts <2 mm) gabbro grades into a gabbro with a grain size of <3 mm. At a distance of approximately 5 m from the contact the grain-sizes are 3 to ≥ 5 mm, typical of the bulk of the intrusion. Plagioclase grain size varies little throughout the intrusion, but the mafic minerals are typically larger in felsic layers than in adjacent mafic layers.

The presence of mm-size plagioclase phenocrysts at the contacts and their sub- to euhedral morphology indicate that plagioclase is a cumulus mineral throughout the crystallisation sequence. Plagioclase oikocrysts with cores that are free from inclusions, and Fe-Ti oxide and olivine enclosed in their margins occur in dark RZ layers.

Olivine phenocrysts in the contact samples occur as glomerocrysts. Olivine is a cumulus mineral throughout the intrusion and, in RZa, euhedral olivine crystals are

abundant. Olivine crystals are enclosed in plagioclase and clinopyroxene in the more mafic layers of RZa. The olivine crystals are euhedral when enclosed in plagioclase and somewhat more rounded when present in clinopyroxene. Olivine crystals are also smaller when enclosed in the oikocrysts. In RZb, olivine represents no more than ~5% of the mode and the crystals are anhedral and in some cases poikilitic.

Fe-Ti oxide is present in the LZ as a post-cumulus mineral and becomes a cumulus mineral near the base of RZa, where it occurs as abundant euhedral grains (Fig. 6b). In LZ, UZ, and most of RZb the Fe-Ti oxide is sub- to anhedral. Euhedral Fe-Ti oxide crystals in RZa are found enclosed in both plagioclase and clinopyroxene. The Fe-Ti oxide consists of magnetite with exsolved ulvöspinel (partly oxidized to ilmenite). However, discrete ilmenite grains are also present (Larson and Magnusson, 1976; Larson, 1980).

Clinopyroxene in the LZ, UZ and RZa occurs interstitial to the other major phases, although it can account for more than 15% of the mode. In these rocks it occurs as oikocrysts up to 3 cm in size. Clinopyroxene is a cumulus mineral in RZb where the crystals are subhedral and accounts for as much as 30% of the mode.

Accessory brownish-red biotite is found associated with Fe-Ti oxide grains and a pale green varitey of biotite is found in the LZ. Euhedral apatite crystals are found in small pockets associated with K-feldspar and as inclusions in clinopyroxene oikocrysts. Apatite becomes a cumulus mineral in RZb. The exact stratigraphic position is poorly constrained because apatite is difficult to identify in the field. K-feldspar is also found intergrown with plagioclase rims.

Analytical methods

Whole rock analyses, by Inductively Coupled Plasma Mass Spectrometry (ICP-MS) were carried out at Actlabs, Canada and follows this laboratorys routines as described below.

Certified rock standards WMG-1 and W2 were analysed as unknowns and rendered accuracies <10% except for Ni, Cu and Zr which were <20%. Samples are prepared and analyzed in a batch system. Each batch contains a blank, certified reference material and replicates. Samples are mixed with a flux of lithium metaborate and lithium tetraborate and fused in an induction furnace. The melt is immediately poured into a solution of 5% nitric acid containing an internal standard, and mixed continuously until completely dissolved (~30 min). The samples are then run for major oxides (Actlabs Code 4 -Litho research) on a combination simultaneous/sequential Thermo Jarrell-Ash ENVIRO II ICP, and trace elements are analysed by a Perkin Elmer SCIEX ELAN 6000 ICP-MS

Mineral major-element compositions were determined using a Zeiss DSM 940 scanning electron microscope with an Oxford Link energy dispersive spectrometer system at the Earth Sciences Center, Göteborg University. Analyses were acquired using an accelerating voltage of 25 kV, a sample current of ~1 nA, and a live counting time of 100 s. The system was calibrated with natural minerals and simple oxide standards. Cobalt was used as a reference standard and to monitor the system drift. Raw counts were reduced using a ZAF correction.

Table 1. *Chilled margin analyses*

Sample #		88	134	146	147*	U1*	204	Avg.	%RSD	294*
SiO_2	wt.%	45.68	45.70	46.41	46.64	46.24	45.98	46.11	0.8	45.95
Al_2O_3	wt.%	15.72	15.77	15.97	15.97	16.00	15.81	15.87	0.8	16.18
Fe_2O_3	wt.%	15.07	15.14	15.47	15.26	15.08	14.01	15.01	3.4	15.10
MnO	wt.%	0.19	0.19	0.20	0.20	0.22	0.19	0.20	5.8	0.18
MgO	wt.%	6.21	6.40	6.64	6.20	5.74	6.11	6.22	4.8	6.96
CaO	wt.%	8.73	8.76	8.73	8.73	8.19	8.69	8.64	2.6	8.63
Na_2O	wt.%	3.06	3.08	2.94	3.01	3.15	2.94	3.03	2.7	2.93
K_2O	wt.%	1.01	1.03	1.01	0.99	1.18	1.07	1.05	6.7	0.90
TiO_2	wt.%	2.39	2.37	2.35	2.40	2.25	2.42	2.36	2.5	2.03
P_2O_5	wt.%	0.41	0.41	0.40	0.41	0.35	0.37	0.39	6.5	0.34
LOI	wt.%	0.26	0	0.18	0.27	1.39	0.22	0.46	–	0.36
Total	wt.%	98.73	98.85	100.30	100.08	99.79	97.81	99.34	–	99.56
Ba	ppm	564	552	533	573	562	586	562	3.2	482
Sr	ppm	390	391	384	400	389	394	391	1.4	401
Sc	ppm	26	26	27	27	27	28	27	2.8	25
V	ppm	247	247	249	252	243	259	249	2.2	242
Cr	ppm	126	128	99	81	77	91	100	21.9	82
Co	ppm	55	57	55	53	55	45	53	8.0	54
Ni	ppm	81	84	84	79	95	71	82	9.7	101
Cu	ppm	110	108	102	67	66	96	91	21.9	49
Zn	ppm	150	168	118	128	156	81	133	23.7	93
Ga	ppm	22	22	21	22	21	21	21	3.1	19
Ge	ppm	1.1	1.6	1.4	1.5	1.5	1.0	1.3	17.8	1.4
Rb	ppm	18	17	16	20	22	19	19	11.0	23
Y	ppm	28.7	28.7	28.2	29.2	28.4	29.7	28.8	1.9	23
Zr	ppm	124	130	128	175	136	132	137	13.7	119
Nb	ppm	6.6	7.3	7.3	7.4	9.4	8.0	8	12.6	5.9
Cs	ppm	0.5	0.5	0.8	1.2	1.0	2.3	1.0	64.1	3.2
La	ppm	16.40	15.90	15.50	16.60	18.50	16.60	16.58	6.2	12.6
Ce	ppm	37.60	36.60	35.70	36.60	40.90	38.50	37.65	4.9	27.8
Pr	ppm	4.98	4.86	4.75	5.43	5.30	5.03	5.06	5.2	4.18
Nd	ppm	22.30	22.80	22.10	23.60	24.90	23.80	23.25	4.5	18.5
Sm	ppm	5.96	5.81	5.72	4.85	5.88	6.06	5.71	7.7	3.72
Eu	ppm	2.31	2.30	2.26	2.17	2.19	2.38	2.27	3.5	1.79
Gd	ppm	6.02	5.95	5.88	4.84	6.30	6.29	5.88	9.2	3.86
Tb	ppm	0.99	0.96	0.96	0.85	0.99	0.99	0.96	5.7	0.68
Dy	ppm	5.60	5.54	5.42	4.83	5.40	5.64	5.41	5.5	3.81
Ho	ppm	1.08	1.09	1.05	1.07	1.06	1.13	1.08	2.6	0.84
Er	ppm	3.17	3.14	3.05	3.00	3.05	3.27	3.11	3.2	2.39
Tm	ppm	0.47	0.47	0.46	0.38	0.45	0.48	0.45	8.1	0.30
Yb	ppm	2.90	2.82	2.73	2.38	2.88	2.97	2.78	7.6	1.90
Lu	ppm	0.42	0.41	0.41	0.41	0.44	0.43	0.42	3.4	0.34
Hf	ppm	3.6	3.7	3.6	3.9	4.0	3.7	3.8	4.4	3.3
Ta	ppm	0.50	0.48	0.47	0.56	0.49	0.50	0.50	6.3	0.39
Tl	ppm	0.13	0.17	0.10	0.22	0.31	0.11	0.17	46.0	0.17
Th	ppm	1.28	1.18	1.15	1.23	1.38	1.22	1.24	6.6	0.79
U	ppm	0.36	0.34	0.33	0.33	0.33	0.35	0.34	3.9	0.25

* Chilled margin from the NUG

Results

Whole rock chemistry

Fine-grained contact samples are thought to approximate the original magma composition (Table 1). They plot in the alkaline basaltic field of Le Maitre et al. (1989). The TiO_2 and Fe_2O_3 contents of the chilled margins are higher ($\sim$2.4 wt.% and $\sim$15 wt.%, respectively), while the phosphorous ($\sim$0.4 wt.% P_2O_5) is similar to the mean of 247 different alkali-olivine basalts (Manson, 1967). REE analyses reveal LREE enrichment (La_n/Lu_n $\sim$3.9–4.3) and a small positive Eu anomaly with concentrations of $\sim$24 to 56 times chondrite values. Spider diagrams (Fig. 7) show some enrichment of LIL elements and Nb-Ta, and Th contents that give distinct negative anomalies in accordance with other CSDG intrusions. Such anomalies are unusal for alkaline basalts and have been explained by chemical interaction between astenosphere derived magma and the lithospheric mantle (Patchett, 1994). The average of these compositions is used below to model crystallization of the intrusion. Two lower contact samples from Norra Ulvön are not included in this average as they contain cumulus olivine (Table 1).

Mineral chemistry

Plagioclase

Average core compositions of plagioclase vary from $\sim An_{67}$ at the base of the intrusion, decreasing continuously to $\sim An_{47}$ at the RZ-UZ contact (Table 2). Plagioclase from the UZ all has average core compositions greater than An_{65} (Fig. 8). Plagioclase from throughout the intrusion shows strong zonation with core to rim variations of >60 An in many samples. Detailed examination of the zonation reveals that many crystals have a small concentric zone of higher An around

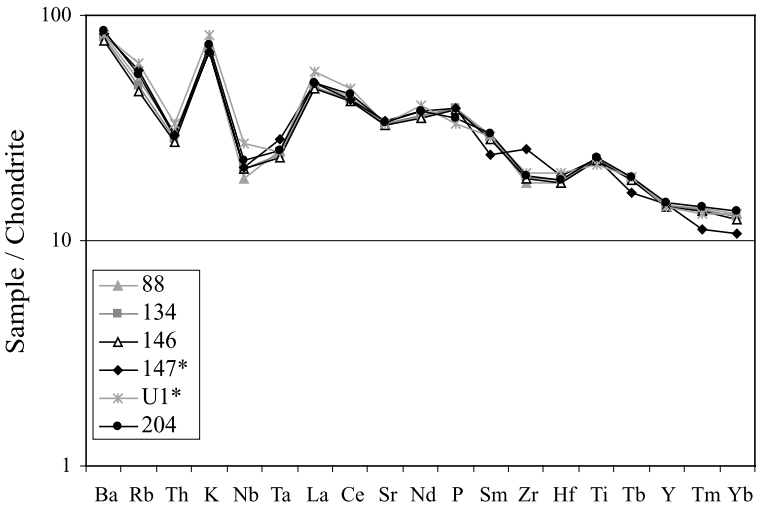

Fig. 7. Spider diagram of samples from lopolith margins of the Ulvö Gabbro Complex (see Table 1). Numbers U1 and 147 are from the studied section at Norra Ulvön

Table 2. *Representative plagioclase analyses (wt.%)*

Height (m)	290(U) core	290(U) rim	240(U) core	240(U) rim	189(D) core	189(D) rim	189(L) core	189(L) rim	148(D) core	148(D) rim	148(L) core	148(L) rim	107(D) core
SiO_2	51.64	61.97	56.42	63.01	55.42	62.17	55.51	61.73	54.84	57.19	54.94	61.76	53.94
Al_2O_3	31.12	24.00	27.77	23.32	28.64	22.93	27.98	23.59	28.98	26.56	28.69	24.34	29.12
FeO	0.29	0.18	0.24	0.13	0.30	0.29	0.34	0.23	0.29	0.19	0.31	0.22	0.30
CaO	13.21	4.78	9.20	3.43	10.18	4.12	9.87	4.61	10.73	8.13	10.38	5.42	10.94
Na_2O	3.73	8.03	5.88	8.68	5.39	7.77	5.35	7.67	5.03	6.24	5.26	7.85	4.93
K_2O	0.22	0.81	0.43	0.90	0.57	1.90	0.57	1.60	0.48	0.71	0.50	0.68	0.48
TiO_2	0.15	bdl	0.10	bdl	0.17	0.24	0.19	0.24	0.11	0.21	0.16	0.08	0.18
Total	100.4	99.8	100	99.5	100.7	99.4	99.8	99.7	100.47	99.24	100.24	100.35	99.9
Si	9.35	11.02	10.15	11.20	9.94	11.14	10.03	11.03	9.86	10.34	9.90	10.94	9.77
Al	6.64	5.03	5.88	4.89	6.05	4.84	5.96	4.97	6.14	5.66	6.09	5.08	6.22
Fe(ii)	0.04	0.03	0.04	0.02	0.04	0.04	0.05	0.03	0.04	0.03	0.05	0.03	0.05
Ca	2.56	0.91	1.77	0.65	1.96	0.79	1.91	0.88	2.07	1.57	2.00	1.03	2.12
Na	1.31	2.77	2.05	2.99	1.87	2.70	1.87	2.66	1.75	2.19	1.84	2.70	1.73
K	0.05	0.18	0.10	0.20	0.13	0.43	0.13	0.36	0.11	0.16	0.11	0.15	0.11
Ti	0.02	0.00	0.00	0.00	0.02	0.03	0.03	0.03	0.01	0.03	0.02	0.01	0.02
Total	19.98	19.94	19.99	19.95	20.02	19.98	19.97	19.97	19.99	19.98	20.01	19.94	20.02
An	65.33	23.58	45.20	16.97	49.39	20.15	48.79	22.60	52.59	40.11	50.65	26.52	53.54
Ab	33.38	71.67	52.28	77.72	47.32	68.78	47.86	68.06	44.61	55.72	46.45	69.52	43.66
Or	1.30	4.76	2.52	5.30	3.29	11.07	3.35	9.34	2.80	4.17	2.90	3.96	2.80

Height (m)	107(D) rim	107(L) core	107(L) rim	57(D) core	57(L) core	57(L) rim	31(D) core	31(D) rim	31(L) core	31(L) rim	7(U) core	7(U) rim
SiO_2	56.89	53.33	56.43	52.46	53.21	63.19	51.57	57.94	51.79	58.04	50.63	58.83
Al_2O_3	27.83	29.30	27.15	30.41	30.15	23.20	31.02	26.06	30.91	26.61	31.99	26.23
FeO	0.38	0.27	0.26	0.29	0.30	0.17	0.41	0.27	0.34	0.29	0.23	0.32
CaO	9.07	11.05	8.99	12.36	11.81	4.18	13.07	7.44	12.85	7.92	14.05	7.53
Na_2O	5.84	4.67	6.13	4.20	4.39	8.04	3.83	6.55	3.98	6.55	3.43	6.47
K_2O	0.82	0.53	0.46	0.32	0.37	0.95	0.32	0.91	0.35	0.58	0.19	0.94
TiO_2	0.14	0.09	0.15	0.12	0.12	0.13	bdl	0.17	0.20	0.20	0.10	0.15
Total	101	99.2	99.6	100.16	100.34	99.85	100.22	99.34	100.41	100.19	100.62	100.48
Si	10.15	9.72	10.19	9.50	9.60	11.20	9.36	10.46	9.38	10.38	9.17	10.49
Al	5.85	6.30	5.78	6.49	6.41	4.84	6.64	5.54	6.60	5.61	6.83	5.51
Fe(ii)	0.06	0.04	0.04	0.04	0.05	0.03	0.06	0.04	0.05	0.04	0.03	0.05
Ca	1.73	2.16	1.74	2.40	2.28	0.79	2.54	1.44	2.49	1.52	2.73	1.44
Na	2.02	1.65	2.15	1.48	1.54	2.76	1.35	2.29	1.40	2.27	1.20	2.24
K	0.19	0.12	0.11	0.07	0.09	0.21	0.07	0.21	0.08	0.13	0.04	0.21
Ti	0.02	0.01	0.02	0.02	0.02	0.02	0.00	0.02	0.03	0.03	0.01	0.02
Total	20.01	20.00	20.02	20.01	19.98	19.85	20.03	20.00	20.03	19.99	20.02	19.96
An	44.00	54.89	43.58	60.76	58.48	21.05	64.13	36.51	62.78	38.70	68.59	36.99
Ab	51.27	41.98	53.77	37.36	39.34	73.26	34.00	58.17	35.19	57.92	30.30	57.51
Or	4.74	3.13	2.65	1.87	2.18	5.70	1.87	5.32	2.04	3.37	1.10	5.50

U Unlayered; *D* dark; *L* light
Cations are calculated on the basis of 32 oxygens

the core and this is enclosed by rims in which the An content decreases rapidly (Fig. 9a). The An content of rims of plagioclase grains adjacent to pockets containing accessory minerals such as K-feldspar, apatite, and allanite grade continuously

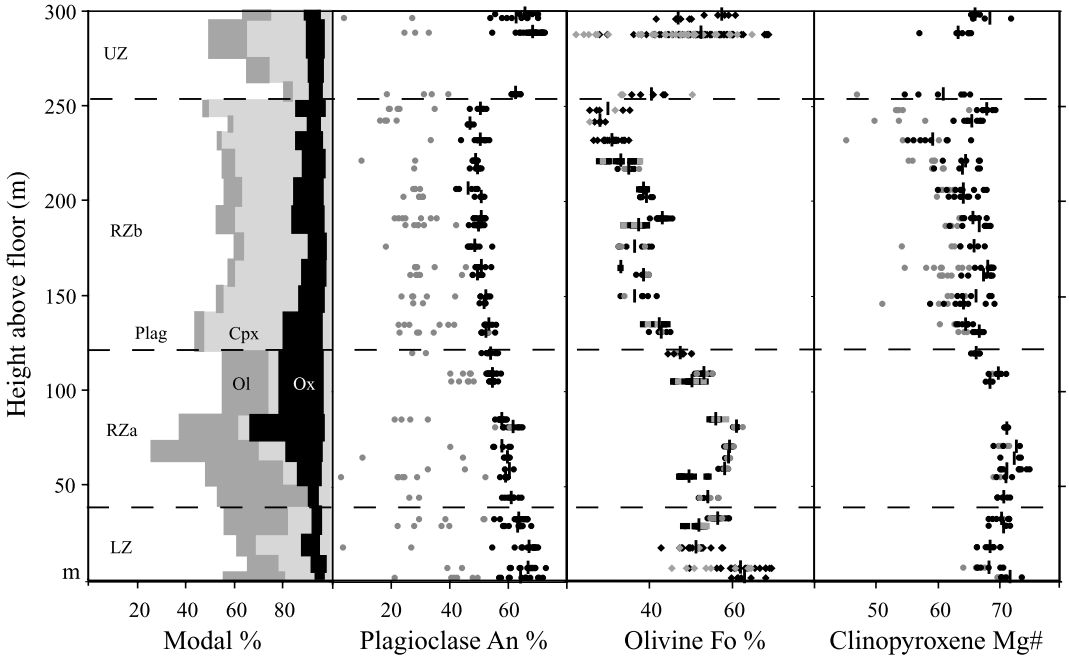

Fig. 8. From left to right: modal mineral variation in the NUG (average of adjacent light and dark layer) in the Norrsand-Sörsand section (Fig. 1). Secondary minerals (not marked in the figure) are e.g. iddingsite, amphibole and chlorite – variation in An content for plagioclase with height above floor. Dark dot: core; Grey dot: rim. Vertical bar: average for cores. – variation in olivine Fo content with height above floor. Dark: core; Grey: rim; Vertical bar: average; Dot: dark layer; Square: light layer; Diamond: unlayered gabbro – variation in Cpx Mg# with height above floor. Dark: core; Grey: rim

into these pockets. Minor-element concentrations in plagioclase vary either sympathetically with An content (TiO_2 and FeO) or antithetically (K_2O). TiO_2 and FeO concentrations vary by a factor ∼2 (from 0.10 to 0.20 and 0.15 to 0.30 wt.% respectively). K_2O is strongly correlated with Na_2O and ranges from less than ∼0.2 in cores to more than ∼1.5 wt.% in some rims.

Olivine

Average olivine core compositions are $\sim Fo_{67}$ at the base of the intrusion and decrease to $\sim Fo_{30}$ at the RZ-UZ contact (Table 3). In the lower 100 m of the intrusion the core compositions show no systematic trend or perhaps a modest reverse trend (Fig. 8). Above the 100 m level the Fo contents decrease rapidly. This trend is most pronounced in the core compositions from RZb in which olivine modal contents are much lower than in the rocks below. Core Fo contents in the UZ also decrease toward the RZ-UZ contact ranging from ∼66 near the upper contact to ∼40 just above the ''sandwich horizon'' (Fig. 8). Olivine core compositions show pronounced variations in adjacent mafic and felsic layers with one pair from lower RZa (∼50 m above the base of the intrusion) having Fo_{58} in the mafic layer and Fo_{48} in the felsic layer. Most olivine grains show limited zonation in Fo content. However samples near the contacts have large anhedral grains that show large ranges in Fo (∼70–20) but are not concentrically zoned. Most minor elements

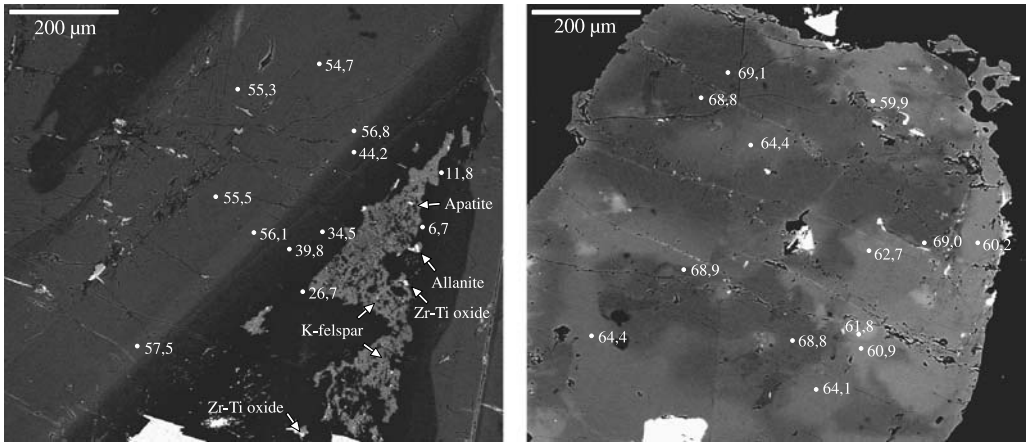

(a) (b)

Fig. 9. (**a**) BSE image of a relatively homogeneous plagioclase core ($An_{54.7–55.5}$) in a sample from a light RZa layer. A thin rim of reverse zonation ($An_{56.8–57.5}$) borders the cumulus plagioclase and is followed by a normally zoned overgrowth ($An_{34.5–44.2}$). The most evolved plagioclase compositions ($An_{6.7–26.7}$) are found within the small interstitial pocket adjacent to late K-feldspar and other accessory minerals. (**b**) BSE image showing variation in composition of a cumulus clinopyroxene from a dark RZb layer. The dark grey areas represent relatively Mg rich clinopyroxene (Mg# = 68.8–69.1), while the lighter areas represent Fe richer compositions (Mg# = 59.9–64.4) most likely influenced by post-cumulus diffusion

are below detection limits (∼0.10 wt.%) in olivine, including NiO. However, CaO concentrations are up to 0.2 and 0.4 wt.% although no stratigraphic trends are evident. MnO is anticorrelated with Fo ranging from ∼0.5 at the upper and lower margins of the intrusion to ∼1.1 wt.% at the RZ-UZ contact.

Clinopyroxene

Major-element concentrations in clinopyroxene show limited variation (Table 4). CaO ranges from ∼20 to 22 wt.% while the Mg# varies from ∼61 to 72. The stratigraphic variation in the Mg# of clinopyroxene show the LZ and RZa having Mg#'s from ∼67 to 72, those in RZb are essentially constant near 65, and analyses from the UZ and near the RZ-UZ contact show a wide range from 61 to 68 (Fig. 8). Any stratigraphic variation in minor elements in clinopyroxene is masked by the strong sector zonation found in the interstitial clinopyroxene of the LZ, RZa, and UZ (Claeson et al., 2007) and a heterogeneous recrystallization found in the RZb (Fig. 9b). For example, Al_2O_3 and TiO_2 concentrations can vary by as much as 2 wt.% between adjacent sectors (a distance of ∼15 microns) in RZa clinopyroxene. Surprisingly, Na_2O concentrations do not reflect the zonations seen in Al_2O_3 and TiO_2 and vary only from ∼0.4 to 0.6 wt.%.

Fe-Ti Oxides

Determination of the igneous compositions of the Fe-Ti oxides is hindered by exsolution and some later oxidation. Reflected-light microscopy reveals that

Table 3. *Representative olivine analyses (wt.%)*

Height (m)	290(U) core	290(U) rim	240(U) core	240(U) rim	189(D) core	189(L) core	189(L) rim	148(D) core	148(D) rim	107(D) core	107(D) rim
SiO_2	37.08	32.79	32.36	32.02	33.62	32.97	33.29	33.73	32.97	35.42	35.08
FeO	28.64	53.84	55.01	55.92	45.36	49.55	50.13	48.04	51.43	37.71	40.68
MnO	0.42	1.07	1.16	1.26	0.84	1.01	0.97	0.84	0.94	0.60	0.68
MgO	39.97	12.76	11.85	10.74	19.59	16.39	16.02	17.79	14.91	26.29	24.20
CaO	0.25	0.28	0.44	0.38	0.31	0.24	0.14	0.29	0.23	0.31	0.12
Total	100.35	100.73	100.82	100.33	99.72	100.16	100.55	100.68	100.48	100.33	100.75
Si	0.94	1.00	1.00	1.00	1.00	0.99	1.00	1.00	1.00	1.00	1.00
Fe(ii)	0.61	1.38	1.42	1.46	1.12	1.25	1.26	1.19	1.30	0.89	0.97
Mn	0.01	0.03	0.03	0.03	0.02	0.03	0.02	0.02	0.02	0.01	0.02
Mg	1.51	0.58	0.55	0.50	0.86	0.74	0.72	0.79	0.67	1.10	1.02
Ca	0.01	0.01	0.01	0.01	0.01	0.01	0.00	0.01	0.01	0.01	0.00
Total	3.07	3.00	3.01	3.01	3.01	3.01	3.00	3.01	3.01	3.17	3.01
Fo	70.80	29.15	27.12	24.92	42.83	36.47	35.76	39.16	33.53	54.76	50.95
Fa	28.46	69.00	70.64	72.79	55.64	61.86	62.78	59.33	64.89	44.07	48.05
Tp	0.42	1.39	1.51	1.66	1.04	1.28	1.23	1.05	1.20	0.71	0.81
Mc	0.32	0.46	0.72	0.63	0.49	0.38	0.22	0.46	0.37	0.46	0.18

Height (m)	107(L) core	107(L) rim	57(D) core	57(D) rim	57(L) core	31(D) core	31(D) rim	31(L) core	31(L) rim	7(U) core	7(U) rim
SiO_2	34.77	34.47	35.74	36.13	34.89	35.84	35.84	35.10	35.54	37.63	34.81
FeO	41.55	43.42	35.04	35.76	42.42	35.53	38.17	39.10	38.46	27.64	42.45
MnO	0.71	0.76	0.57	0.52	0.78	0.54	0.69	0.65	0.66	0.29	0.80
MgO	22.91	21.71	28.57	27.83	22.40	27.90	25.94	25.16	25.34	34.73	22.72
CaO	0.28	0.21	0.21	0.13	0.30	0.28	0.19	0.30	0.29	0.30	0.17
Total	100.22	100.56	100.12	100.36	100.78	100.10	100.83	100.31	100.30	100.58	100.95
Si	1.00	1.00	0.99	1.00	1.00	1.00	1.00	1.00	1.00	1.00	1.00
Fe(ii)	1.00	1.05	0.81	0.83	1.02	0.83	0.89	0.93	0.91	0.61	1.02
Mn	0.02	0.02	0.01	0.01	0.02	0.01	0.02	0.02	0.02	0.01	0.02
Mg	0.98	0.94	1.18	1.15	0.96	1.16	1.08	1.06	1.07	1.38	0.97
Ca	0.01	0.01	0.01	0.00	0.01	0.01	0.01	0.01	0.01	0.01	0.01
Total	3.01	3.01	3.01	3.00	3.01	3.01	3.00	3.01	3.00	3.01	3.01
Fo	48.93	46.54	58.66	57.64	47.80	57.71	54.17	52.77	53.35	68.61	48.22
Fa	49.78	52.22	40.36	41.55	50.79	41.23	44.72	46.01	45.42	30.64	50.55
Tp	0.86	0.93	0.67	0.61	0.95	0.63	0.82	0.77	0.79	0.33	0.96
Mc	0.43	0.32	0.31	0.19	0.46	0.42	0.29	0.45	0.44	0.43	0.26

U Unlayered; *D* dark; *L* light
Cations are calculated on the basis of 4 oxygens

ulvöspinel and magnetite are intimately inter-grown, while ilmenite can be found in several textural varieties. These are as discrete crystals, larger crystals bordering magnetite, and lamella and patchy domains within magnetite. Discrete ilmenite is most abundant at the top and bottom of the intrusion. This is the only ilmenite type

Table 4. *Representative clinopyroxene analyses (wt.%)*

Height (m)	290(U) core	240(U) core	240(U) rim	189(D) core	189(D) rim	189(L) core	189(L) rim	148(D) core	148(D) rim	148(L) core	148(L) rim	107(D) core	107(L) core	57(D) core	57(L) core	31(D) core	31(L) core	7(U) core
SiO_2	49.99	50.95	50.95	51.73	51.58	51.20	50.81	51.94	51.60	51.03	51.24	51.80	51.31	51.34	50.60	51.58	51.10	51.95
TiO_2	1.02	1.63	0.64	1.03	1.01	1.11	1.05	1.18	1.12	1.34	0.27	1.11	1.43	1.26	1.74	1.44	1.67	1.10
Al_2O_3	3.56	2.66	1.57	1.86	1.70	2.08	1.94	2.31	2.20	2.64	0.80	2.23	2.58	2.34	3.67	2.30	2.65	2.13
FeO	11.20	12.13	15.98	12.17	12.65	12.20	13.17	11.21	12.26	11.11	16.14	10.90	10.86	10.11	10.33	10.31	10.84	9.91
MnO	0.24	0.21	0.45	0.26	0.29	0.29	0.33	0.18	0.29	0.31	0.43	0.26	0.31	0.19	0.25	0.27	0.23	0.16
MgO	11.64	12.69	8.89	12.33	12.43	12.20	11.74	13.68	12.47	13.16	9.46	13.60	13.26	13.70	13.27	13.76	13.06	13.40
CaO	21.16	20.20	21.22	20.75	20.65	20.76	20.15	20.02	20.43	20.17	21.00	20.45	20.61	20.49	20.72	20.62	20.62	21.59
Na_2O	0.56	0.48	0.58	0.42	0.57	0.50	0.42	0.42	0.49	0.56	0.44	0.50	0.47	0.65	0.28	0.45	0.70	0.62
Total	99.37	100.95	100.28	100.56	100.88	100.33	99.60	100.94	100.86	100.32	99.79	100.85	100.83	100.09	100.86	100.72	100.86	100.84
Si	1.90	1.91	1.96	1.94	1.94	1.93	1.94	1.93	1.93	1.91	1.98	1.93	1.91	1.92	1.88	1.92	1.91	1.93
Ti	0.03	0.05	0.02	0.03	0.03	0.03	0.03	0.03	0.03	0.04	0.01	0.03	0.04	0.04	0.05	0.04	0.05	0.03
Al	0.16	0.12	0.07	0.08	0.08	0.09	0.09	0.10	0.10	0.12	0.04	0.10	0.11	0.10	0.16	0.10	0.12	0.09
Cr	0.00	0.00	0.00	0.00	0.00	0.00	0.00	0.00	0.00	0.00	0.00	0.00	0.00	0.00	0.00	0.00	0.00	0.00
Fe(ii)	0.36	0.38	0.51	0.38	0.40	0.38	0.42	0.35	0.38	0.35	0.52	0.34	0.34	0.32	0.32	0.32	0.34	0.31
Mn	0.01	0.01	0.01	0.01	0.01	0.01	0.01	0.01	0.01	0.01	0.01	0.01	0.01	0.01	0.01	0.01	0.01	0.01
Mg	0.66	0.71	0.51	0.69	0.70	0.69	0.67	0.76	0.70	0.74	0.55	0.75	0.74	0.76	0.74	0.76	0.73	0.74
Ca	0.86	0.81	0.87	0.84	0.83	0.84	0.82	0.80	0.82	0.81	0.87	0.82	0.82	0.82	0.83	0.82	0.82	0.86
Na	0.04	0.03	0.04	0.03	0.04	0.04	0.03	0.03	0.04	0.04	0.03	0.04	0.03	0.05	0.02	0.03	0.05	0.04
K	0.00	0.00	0.00	0.00	0.00	0.00	0.00	0.00	0.00	0.00	0.00	0.00	0.00	0.00	0.00	0.00	0.00	0.00
Total	4.01	4.01	4.01	4.00	4.02	4.01	4.01	4.00	4.01	4.01	4.01	4.01	4.01	4.02	4.00	4.01	4.01	4.01

U Unlayered; *D* dark; *L* light

Cations are calculated on the basis of 6 oxygens

interpreted to have crystallized from the magma. In an effort to reintergrate the oxides, analyses were conducted using a beam raster mode to integrate 50 μm^2 (Table 5). An insufficient number of samples were analyzed to assess stratigraphic

Table 5. *Representative Fe-Ti oxide analyses (wt.%)*

Height (m)	256(U)	232(U)	189(D)	189(L)	107(D)	107(L)	7(U)
SiO_2	0.15	0.16	0.16	0.18	0.23	bdl	bdl
TiO_2	22.6	21.11	23.32	21.97	22.06	21.84	22.61
Al_2O_3	1.79	2.27	2.19	2.55	2.8	2.34	2.29
V_2O_5	0.74	0.48	1.16	0.91	1.5	0.95	0.74
FeO	71.67	70.39	68.45	70.97	70.09	69.91	69.46
MnO	0.66	0.58	0.51	0.51	0.45	0.58	0.72
MgO	0.24	0.19	1.02	0.72	1.41	1.1	0.77
Total	97.85	95.18	96.81	97.81	98.54	96.72	96.59
Si	0.05	0.05	0.05	0.06	0.06	0.00	0.00
Ti	5.05	4.84	4.84	4.88	4.83	4.89	5.09
Al	0.63	0.82	0.82	0.88	0.96	0.82	0.80
V	0.18	0.12	0.12	0.21	0.35	0.23	0.18
Fe(ii)	17.82	17.94	17.94	17.52	17.07	17.42	17.39
Mn	0.17	0.15	0.15	0.13	0.11	0.15	0.18
Mg	0.11	0.08	0.08	0.31	0.61	0.49	0.34
Total	24	24	24	24	24	24	24

U Unlayered; *D* dark; *L* light
Cations are calculated on the basis of 32 oxygens and normalised to a total of 24

Table 6. *Representative biotite analyses (wt.%)*

Height (m)	256(U)	232(U)	189(D)	189(L)	107(D)	107(L)	7(U)
SiO_2	35.19	34.95	36.06	36.86	36.72	36.59	35.31
TiO_2	6.63	6.57	8.22	6.34	7.87	6.24	7.37
Al_2O_3	12.69	13.08	13.30	13.64	13.72	13.31	13.67
FeO	26.12	24.17	17.84	18.49	15.65	16.48	17.00
MgO	6.36	7.47	11.23	12.02	12.85	13.13	11.72
Na_2O	0.75	0.38	0.72	0.72	0.62	0.65	bdl
K_2O	9.03	9.03	9.00	8.94	9.02	9.13	9.19
Total	96.77	95.65	96.37	97.01	96.45	95.53	94.26
Si	5.51	5.48	5.43	5.51	5.45	5.52	5.42
Ti	0.78	0.77	0.93	0.71	0.88	0.71	0.85
Al	2.34	2.42	2.36	2.40	2.40	2.37	2.47
Fe(ii)	3.42	3.17	2.25	2.31	1.94	2.08	2.18
Mg	1.48	1.75	2.52	2.68	2.85	2.95	2.68
Na	0.23	0.12	0.21	0.21	0.18	0.19	0.00
K	1.80	1.81	1.73	1.70	1.71	1.76	1.80
Total	15.56	15.50	15.43	15.53	15.41	15.57	15.40

U Unlayered; *D* dark; *L* light
Cations are calculated on the basis of 22 oxygens

variation in the oxides. However, comparison of oxides in adjacent layers reveals that magnetite in the mafic layers is richer in V_2O_5, MgO, TiO_2, and Al_2O_3 than that in felsic layers.

Biotite

The Mg#'s of biotite are lower in RZb as expected, based on olivine and clinopyroxene compositions. However, Mg#'s of biotite elsewhere are more variable perhaps related to the smaller modal abundance outside of RZb (Table 6). Primary biotite is deep red in color, has up to ~8 wt.% TiO_2, and is spatially associated with oxide grains. The pale green biotite is poor in TiO_2 (~0.2 wt.%).

Discussion

We begin the discussion by briefly reviewing how some of the layering features seen in the Ulvö Gabbro Complex are thought to have formed in other layered intrusions. We then present a model for the construction of the NUG based on stratigraphic variations in mineral proportions and compositions.

Origin of layering features in the Ulvö Gabbro Complex

The layering features developed in the Ulvö Gabbro Complex provide evidence of the processes that governed the segregation of the crystals from the liquid. Our object in this overview of how the intrusions formed is to evaluate the features seen in the light of how similar features are proposed to have formed in other layered intrusions. By doing so, a basis is provided for understanding what parameters of the system are most important in the development of layering. The proposed processes responsible for the various layering features fall into three general categories (see reviews in Parsons (1987) and Cawthorn (1996)): (1) Nucleation-controlled features are those created by variations in nucleation rates due to fluctuations in intensive parameters, e.g. temperature, pressure and chemistry. (2) Primary accumulation features are those generated by gravitational sorting, such as graded beds, or by the actions of magmatic currents such as unconformities. (3) Post-cumulus features are those produced in the partially consolidated crystal mush such as diffusional homogenization and mineral alignment by compaction. Most of the layering features documented in the Ulvö Gabbro Complex have elsewhere been explained by mechanisms that fall into two and sometime all three categories. In the discussion below we note the preferred category(ies), concerning the Ulvö Gabbro Complex, for each feature in square brackets at the end of each paragraph.

The rhythmic layering consists mainly of differences in modal proportions but differences of grain size and texture can be used to interprete the origin of layering. Cumulus mineral grains, especially olivine and oxides, are usually smaller in the mafic layers of the Ulvö Gabbro Complex in which their modal proportion is relatively high. This is most evident for euhedral olivine crystals enclosed in oikiocrysts of clinopyroxene which are much smaller in mafic layers than olivine crystals in felsic layers. This excludes a process where gravitational settling only was responsible for the layering. Naslund and McBirney (1996) argued that the

inverse correlation of grain size to modal abundance is expected if the layering process was nucleation-controlled. However, for the Ulvö Gabbro Complex the relatively high amount of postcumulus crystallization in felsic layers (Larson, 1980) explains the larger and less euhedral grains of olivine and oxide observed in these layers [3].

Mineral foliations in layered intrusions can be generated during primary deposition from magmatic currents (e.g. McBirney and Nicolas, 1997) or via compaction of a crystal mush (Wager et al., 1960; Jackson, 1961; Richter and McKenzie, 1984; McKenzie, 1985, 1987; Sparks et al., 1985; Shirley, 1986). The well-layered sections of the Ulvö Gabbro Complex have a strong foliation and locally a lineation defined by plagioclase. Since lineation is mainly observed in connection to slump structures, it is likely formed by movements in the crystal mush, e.g. by slumping. There is little evidence for grain deformation, which might be taken to indicate that compaction was not responsible for the fabric. However, grain-boundary migration can allow extremely well-foliated rocks to form without inducing discernible strain (Meurer and Boudreau, 1998) [2, 3].

Trough structures similar to those seen in the Ulvö Gabbro Complex (Fig. 4c) are found in the Skaergaard intrusion. Wager and Brown (1968) attributed them to intermittent density currents during the later stages of crystallization. They have also been attributed to compaction of the crystal pile (Sonnenthal, 1992; McBirney and Nicolas, 1997). The thickening of the layers in most of the trough structures, and the higher concentrations of dark minerals near the axis of these troughs, sometimes forming lenses, both seem more consistent with erosion and deposition by density currents. However, a few of the trough structures which are of low amplitude appear to be connected and lack significant concentration of mafic minerals to the trough bottom, indicating that they might be folds and related to the deformation of the crystal pile during compaction and/or slumping [2, 3].

Strata-bound anorthositic lenses (Fig. 6b) form ''fragmental layers'' that might provide evidence of magmatic transport and deposition of the fragments (Irvine et al., 1998). Alternatively, they might be formed via a replacement process in the crystal pile (McBirney, 1987). However, in the Ulvö Gabbro Complex the shapes of the lenses, the draping of layers around these, and lack of evidence for replacement processes seem more consistent with an origin by magmatic transport processes [2].

Slump structures (Fig. 4a) are mostly restricted to a discrete stratigraphic horizon. As their name implies these features are generally interpreted as the result of movement and deformation within the crystal mush (e.g. McCallum et al., 1980; Meurer and Boudreau, 1996). Pending additional work on these features, no alternate categories of explanation seem viable [3].

Plagioclase-rich segregations with mafic margins (Fig. 6a) look like those in the Skaergaard intrusion that are interpreted as the product of replacement through H_2O infiltration metasomatism (Irvine, 1980, 1987) or related to gabbroic pegmatoid formation (e.g. Sonnenthal, 1992; Larsen and Brooks, 1994). They have also been interpreted as a product of deformation of the crystal pile that resulted in the segregation of liquids into zones of minimum stress (Naslund and McBirney, 1996). There is no clear evidence for deformation or affiliation to pegmatites for

these features in the Ulvö Gabbro Complex. Pending additional work on these features, no alternate categories of explanation seem viable [3].

Coarse-grained gabbro pegmatites are common features in layered gabbros (e.g. Cawthorn, 1996). Gabbroic pegmatoids are generally ascribed to the concentration of volatiles in the crystal pile (e.g. Puffer and Horter, 1993). Models include filter pressing of interstitial liquids in a compacting cumulus pile (Anderson et al., 1984; Greenough and Dostal, 1992; Carman, 1994; Philpotts et al., 1996; Greenough et al., 1999; Puffer and Volkert, 2001) and fluid induced partial re-melting of cumulates (e.g. Boudreau, 1999).

In the Ulvö Gabbro Complex patchy gabbroic pegmatoids are common in areas characterized by slumping and disturbed layering. In the NUG these pegmatoids are also localized at the RZ-UZ contact (''sandwich horizon''). Preliminary results (Landersjö, 2006) indicate that pegmatoids in the Ulvö Gabbro Complex are consistent with a replacement origin since the content of incompatible elements is similar to that in the host gabbro [3].

Construction of the Norra Ulvön Gabbro

The Norra Ulvön transect is a complete cross-section of a magma chamber and allows us to construct a detailed stratigraphy (Fig. 8). The crystallization sequence of the cumulus minerals is olivine and plagioclase followed by Fe-Ti oxides and finally clinopyroxene. The most evolved minerals are found ~50 m below the upper contact. This ''Sandwich Horizon'' represents the meeting between the upward growing floor zones which constitutes approximately 5/6 of the entire thickness and the downward growing roof zone (UZ). Examination of the average core compositions of the cumulus minerals provides insight into the details of the fractional-crystallization processes.

The trend of decreasing An content in the core compositions of plagioclase is consistent with a simple differentiation trend of a single batch of magma, with the final liquid solidifying at ~250 m above the floor of the intrusion. The much higher An contents above the Sandwich Horizon, along with the interstitial habits of the oxides and clinopyroxene in the UZ, suggest that significant downward growth from the roof ceased at, or before, the complete upward growth of LZ from the floor. This is in contrast to intrusions such as the Skaergaard that have stratigraphically equivalent units in both the floor upward and the roof downward growth zones (McBirney, 1989).

The olivine core compositions generally appear to support an interpretation of simple fractional crystallization. However, a weak increasing trend in the Mg# from the base of the intrusion to approximately 100 m is present. Similar reverse trends have been reported at the bases of other layered intrusions and are explained as a consequence of a decreasing amount of crystallized interstitial liquid with height (e.g., Stillwater Complex, Duluth Complex; Raedeke and McCallum, 1984; Chalokwu and Grant, 1987). As an insulating zone of cumulates slows the rate of heat transfer through the floor, the amount of liquid that crystallizes within the cumulates decreases. Larger amounts of crystallized interstitial liquid can diffusively homogenize with the core of the cumulus minerals and substantially lowering their Mg/Fe ratios (Barnes, 1986). This process explains the modest reverse

trends present in olivine at the base of the intrusion. Similarly, the evolved compositions of the olivine immediately above the Sandwich Horizon likely reflect equilibration with evolved liquids driven upward by compaction.

Clinopyroxene does not become a cumulus mineral until the base of RZb, after nearly 50% of the stratigraphic section was constructed, if the interpretation of the UZ growth discussed above is correct. The Mg# of the interstitial clinopyroxene shows a gradual increase from the base of the intrusion and a decrease to RZb that is similar to the trend of the olivine. Cores of cumulus clinopyroxene grains in RZb show an irregular but decreasing trend in their Mg#. There is a slight increase in the Mg# of the clinopyroxene just below the SH that is antithetical to trends in the olivine cores. It should be noted that the cumulus clinopyroxene grains in RZb have an unusual patchy zonation (see above) that obscures our ability to reliably select core compositions in some instances. The limited range in the clinopyroxene Mg#s in RZb is similar to the modest range seen in the plagioclase An content and may indicate that limited fractionation took place in RZb.

The proposed model can be tested using a thermodynamic model for liquid fractionation combined with a model for the incorporation of a crystallized liquid fraction within the cumulates (cf. Meurer and Boudreau, 1998). We constructed such a model using MELTS to model the perfect fractional crystallization of the average chilled margin composition (Ghiorso and Sack, 1995; Asimow and Ghiorso, 1998; Table 1). Model parameters include: a crystallization pressure of 1 kb, an initial water content of 0.75 wt.%, and an oxygen fugacity of FMQ-1. It was not possible to match the plagioclase anorthite- and olivine forsterite-contents observed in marginal samples using melts via any combination of water content and oxygen fugacity. The values used provide the same relative difference between the Fo and An contents as found in the rocks. Additionally, the oxygen fugacity was constrained so that the spinel phase saturated before clinopyroxene. The model was run with 3 °C steps and calculated crystallization of the system up to 88% solidified (and then became unstable). The MELTS model predicts early crystallization of ~3% olivine before plagioclase joins the crystallizing assemblage. An Fe-Ti oxide phase (predominantly ulvöspinel) saturates after ~22% crystallization, clinopyroxene after ~28%, and apatite saturates after ~65% fractional crystallization.

We used the perfect fractional crystallization model to calculate the stratigraphic variation in modal proportions by including crystallized interstitial liquid in the solid assemblage (Fig. 10a). After ~5% fractional crystallization, a liquid component with the composition of the remaining liquid was added. The solid assemblage produced by the liquid component is that of equilibrium crystallization of that liquid. The first 25 m of the LZ and UZ contain 45% crystallized interstitial liquid and the remainder of these zones contains 40% crystallized interstitial liquid. The lower portion of RZa was modeled as containing 35% crystallized interstitial liquid and the rest of the intrusion with 30%. Because magma from the main chamber is consumed both by fractional crystallization and by incorporation into the crystal pile, the entire stratigraphic thickness (300 m) is constructed after ~70% fractional crystallization. The most evolved magma produced is accommodated as crystallized interstitial liquid in the cumulates just below the SH. The MELTS-based

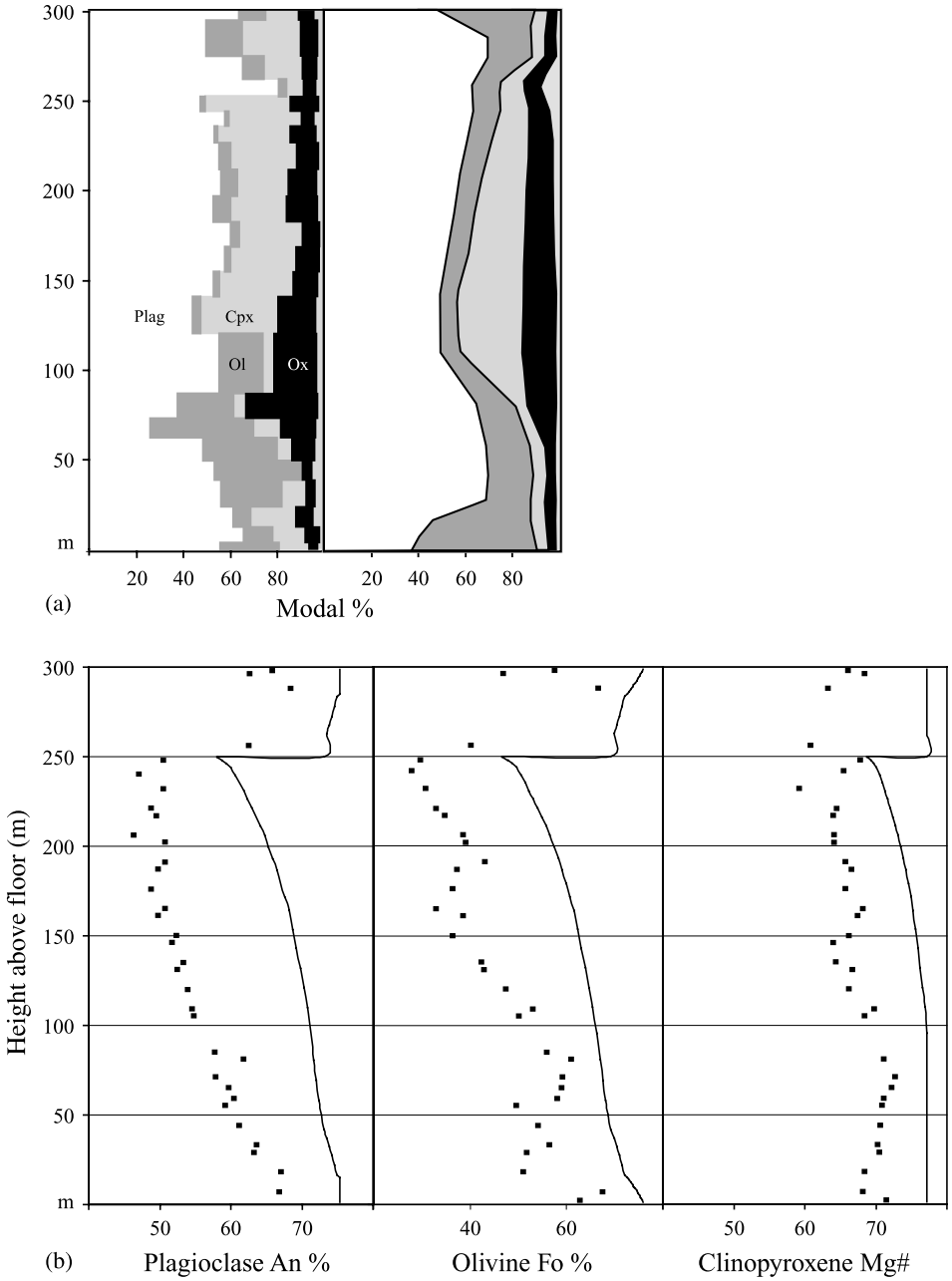

Fig. 10. (**a**) Comparision of modal stratigraphic variation in NUG as calculated from thin sections (left) with calculated stratigraphic variation in modal proportions using perfect fractional crystallization and including crystallized interstitial liquid in the solid assemblage in the calculations (right; see text). (**b**) Comparison of the observed core compositions and predicted mineral compositions, from MELTS calculations (see text)

model reasonably predicts the stratigraphic positions for the saturation of oxide and clinopyroxene. However, the model predicts an over-abundance of olivine near the base of the intrusion and its persistence in significant amounts into RZb, after

clinopyroxene saturation, which are not observed. The model also does not predict the local enrichments in oxides seen shortly after oxide saturates.

Comparison of the observed core compositions and predicted mineral compositions, from MELTS, shows that the observed compositions are systematically more evolved (Fig. 10b). This is not a surprise since we could not match the compositions of the marginal samples. We interpret this shift to reflect the fact that MELTS is not well calibrated for alkali-olivine basalt compositions. In all instances it can be seen that if the model curves are shifted such that their initial compositions match the core compositions at the base of the intrusion, then the model curves fit the data better. However, the olivine core compositions evolve more rapidly than predicted and the plagioclase core compositions evolve more rapidly initially and then more slowly in RZb. The more extensive evolution of the olivine compared to the model predicitions, suggests that the real core compositions have undergone diffusional homogenization with evolved overgrowths – also indicated by the lack of core-rim variation as seen in plagioclase.

Conclusion

The main goal of this work is to characterize and assess the origins of the layering features of the Ulvö Gabbro Complex in general and to examine the construction of the NUG in particular. The most striking feature of the Ulvö Gabbro Complex is the complexity of the layering features observed given the relatively short crystallization and cooling history expected for such small and shallowly emplaced intrusions. Almost a complete set of layering features otherwise observed in much larger intrusions are represented. Our survey of the potential origins of these features does suggest that sedimentary type, cumulus processes are important; however, they are likely modified by a variety of postcumulus processes. We have not found any obvious results pointing towards nucleation controlled processes to explain the rhythmic layering so far. More detailed study of any given feature is required to determine the relative importance of each set of mechanisms.

The NUG was constructed asymmetrically with the roof downward growth ceasing after only 33% of the intrusion had formed. The end of the roof downward growth marks the onset of significant modal layering. The fractionation trends defined by the cumulus minerals are best explained by closed-system fractional crystallization. This interpretation is supported by our ability to model the modal variations in the intrusion as a closed system. Although the observed compositions are systematically more evolved than those predicted by MELTS, the general trends are similar. Some of the olivine compositions in RZb are more evolved than expected from the MELTS model and this likely reflects variable amounts of re-equilibration with evolved overgrowths. We plan to refine this model by including bulk rock chemistry across the entire stratigraphy to better estimate the amount of crystallized interstitial liquid.

The Ulvö Gabbro Complex provides an ideal locality to enhanceour understanding of cumulus processes in layered intrusions. The intrusions: (1) have a well-constrained parental liquid composition, (2) cooled rapidly, and (3) have seen no later metamorphism. They therefore provide a fertile site for additional research.

Acknowledgement

This study was financially supported by grants given to SÅL by the Geological Survey of Sweden (03-1211/99) and the Swedish Research Council (60-1159/2002). Valuable criticism was given by W. Bohrson, A.E. Boudreau, and C. Tegner.

References

Anderson AT, Swihart GH, Artoli G, Geiger CA (1984) Segregation vesicles, gas filter pressing, and igneous differentiation. J Geol 92: 55–72

Asimow PD, Ghiorso MS (1998) Algorithmic modifications extending MELTS to calculate subsolidus phase relations. Am Mineral 83: 1127–1131

Barnes SJ (1986) The effect of trapped liquid crystallization on cumulus mineral compositions in layered intrusions. Contrib Mineral Petrol 93: 524–531

Boudreau A (1999) Fluid fluxing of cumulates: the J–M reef and associated rocks of the Stillwater complex, Montana. J Petrol 40: 755–772

Carman MF Jr (1994) Mechanisms of differentiation in shallow mafic alkaline intrusions, as illustrated in the Big Bend area, western Texas. J Volcanol Geoth Res 61: 1–44

Cawthorn RG (1996) Layered intrusions. In: Cawthorn RG (ed) Developments in Petrology 15, Amsterdam, Elsevier Science B.V, 531 pp

Chalokwu CI, Grant NK (1987) Re-equilibration of olivine with trapped liquid in the Duluth Complex, Minnesota. Geology 15: 71–74

Claeson DT, Meurer WP, Hogmalm KJ, Larson SÅ (2007) Using LA-ICPMS Mapping and Sector Zonation to Understand Growth and Trace-Element Partitioning in Sector-Zoned Clinopyroxene Oikocrysts from the Norra Ulvö Gabbro, Sweden. J Petrol 48: 711–728

Dellvik CA (1875) Report. Geologiska Föreningens i Stockholm Förhandlingar 7: 189

Greenough JD, Dostal J (1992) Cooling history and differentiation of a thick North Mountain Basalt flow (Nova Scotia, Canada). Bull Volcanol 55: 63–73

Greenough JD, Lee C-Y, Fryer BJ (1999) Evidence for volatile-influenced differentiation in a layered alkali basalt flow, Penghu Islands, Taiwan. Bull Volcanol 60: 412–424

Eckerman H (1938) The Anorthosite and Kenningite of the Nordingrå-Rödö region. Geologiska Föreningens I Stockholm Förhandlingar 60: 243–284

Eckerman H (1946) Contribution to the knowledge of the Jotnian rocks of the Nordingrå-Rödö region XII–XXII. Geologiska Föreningens i Stockholm Förghandlingar 68: 412–418

Eckerman H (1947) Contributions to the knowledge of the Jotnian rocks of the Nordingrå-Rödö region XIV–XXII. Geologiska Föreningens I Stockholm Förhandlingar 69: 163–183

Erdmann A (1846) Om de i Sverige förekommande bergarter som föra hornblende eller augit. Kungl. Vetenskapsakeademins Förhandlingar, p 271

Erdmann A (1848) Om den titanhaltiga jernmalmen från Ulföarne. Öfversikt af Vetenskaps Akademiens Förhandlingar

Ghiorso MS, Sack RO (1995) Chemical mass transfer in magmatic processes. IV. A revised and internally consistent thermodynamic model for the interpolation and extrapolation of liquid-solid equilibria in magmatic systems at elevated temperatures and pressures. Contrib Mineral Petrol 119: 197–212

Gorbatschev R, Solyom Z, Johansson I (1979) The central Scandinavian dolerite group in Jämtland, Central Sweden. Geologiska Föreningens i Stockholm Förhandlingar 101: 177–190

Greenough JD, Lee C-Y, Fryer BJ (1999) Evidence for volatile-influenced differentiation in a layered alkali basalt flow, Penghu Islands, Taiwan. Bull Volcanol 60: 412–424

Högbohm AG (1893) Om postarkäiska eruptiver inom det svensk-finska urberget. Geologiska Föreningens i Stockholm Förhandlingar 15: 209–240
Högbohm AG (1909a) Precambrian geology of Sweden. Bulletine of the Geological Institution, University of Upsala X: 1–80
Högbohm AG (1909b) The igneous rocks of Ragunda, Alnö, Rödö and Nordingrå. Geologiska Föreningens i Stockholm Förhandlingar 31: 347–375
Hogmalm KJ, Söderlund, U, Larson SÅ, Meurer WP, Hellström FA, Claeson DT (2006) The Ulvö Gabbro Complex of the 1.27–1.25 Ga Central Scandinavian Dolerite Group (CSDG): intrusive age, magmatic setting and metamorphic history. GFF 128: 1–6
Irvine TN (1980) Magmatic infiltration metasomatism, double-diffusive fractional crystallization, and adcumulus growth in the Muskox intrusion and other layered intrusions. In: Hargraves RB (ed) Physics of magmatic processes. Princeton, N.J., Princeton University Press, pp 325–383
Irvine TN (1987) Layering and related structures in the Duke Island and Skaeragaard intrusions; similarities, differences, and origins. In: Parsons I (ed) Origins of igneous layering. Boston: Reidel, pp 185–245
Irvine TN, Andersen JCØ, Brooks CK (1998) Included blocks (and blocks within blocks) in the skaergaard intrusion: geologic relations and the origins of rhythmic modally graded layers. Geol Soc Am Bull 110: 1398–1447
Jackson ED (1961) Primary textures and mineral associations in the Ultramafic zone of the Stillwater complex, Montana. U.S. Geol Sur Prof Paper 358: 1–106
Landersjö L (2006) Geochemical trends and character of pegmatoids in the Ulvö Gabbro Complex. Earth Sciences Centre, Göteborg University, B484, 2006, 25 pp
Larsen RB, Brooks CK (1994) Origin and evolution of pegmatites in the Skaergaard intrusion, East Greenland. J Petrol 35: 1651–1680
Larson SÅ (1973) Igneous layering in the Ulvö dolerite, Ångermanland, central Sweden. Geologiska Föreningens i Stockholm Förhandlingar 95: 407–409
Larson SÅ (1980) The layered Ulvö dolerite complex, Nordingrå, central Sweden. Geologiska Institutionen, Göteborgs Universitet/Chalmers Tekniska Högskola, Publ. A 36, 213 pp
Larson SÅ, Magnusson K-Å (1976) The magnetic and chemical character of Fe-Ti oxides in the Ulvö dolerite, central Sweden. Sveriges Geologiska Undersökning, C723, 29 pp
Larson SÅ, Magnusson K-Å (1979) A gravity investigation of the dolerite area on the coast of Ångermanland, Sweden. Geologiska Föreningens i Stockholm Förhandlingar 101: 1–16
LeMaitre RW, Bateman P, Dudek A, Keller J, Lameyre Le Bas MJ, Sabine PA, Schmid R, Sorensen H, Streckeisen A, Wooley AR, Zanettin B (1989) A classification of igneous rocks and glossary of terms. Oxford, Blackwell, 193 pp
Lindh A (1973) Relations between iron-titanium oxide minerals and silicate minerals in a dolerite intrusion. Neues Jahrbuch Mineral Abh 120: 31–50
Lundbohm H (1893) Om berggrunden i Vesternorrlands kusttrakter. Geologiska Föreningens i Stockholm Förhandlingar 15: 321–326
Lundqvist Th (1990) Beskrivning till berggrundskartan över Västernorrlands län (English summary). Sveriges Geologiska Undersökning Ba 31, 429 pp
Lundqvist Th, Samuelsson L (1973) The differentiation of a dolerite at Nordingrå, central Sweden. Sveriges Geologiska Undersökning C 692
Magnusson K-Å, Larson SÅ (1977) A paleomagnetic investigation of the Ulvö dolerite, Ångermanland, central Sweden. Lithos 10: 205–211
Manson V (1967) Geochemistry of basaltic rocks: major elements. In: Hess H, Poldervaart A (eds), Basalts. New York, John Wiley and Sons, pp 215–269

McBirney AR, Nicholas A (1997) The Skaergaard layered series, Part II: Magmatic flow and dynamic layering. J Petrol 38: 569–580
McBirney AR (1989) The Skaergaard layered series; I, Structure and average compositions. J Petrol 30: 363–397
McCallum IS, Raedeke LD, Mathez EA (1980) Investigations of the Stillwater Complex; Part 1, Stratigraphy and structure of the Banded Zone. Am J Sci 280: 59–87
McKenzie DP (1985) The extraction of magma from the crust and mantle. Earth Planet Sci Lett 74: 81–91
McKenzie DP (1987) The compaction of igneous and sedimentary rocks. J Geol Soc London 144: 293–307
Meurer WP, Boudreau AE (1996) Petrology and mineral compositions of the middle banded series of the Stillwater Complex, Montana. J Petrol 37: 583–607
Meurer WP, Boudreau AE (1998) Compaction of igneopus cumulates; Part II, Compaction and development of igneous foliations. J Geol 106: 293–304
Mogensen F (1946) A ferro-ortho-titanate ore from Södra Ulvön. Geologiska Föreningens i Stockholm Förhandlingar 68: 578–588
Naslund HR, McBirney AR (1996) Mechanisms of formation of igneous layering. In: Cawthorn RG (ed), Layered Intrusions. Amsterdam, Elsevier Science B.V., pp 1–43
Parsons I (ed) (1987) Origins of igneous layering, NATO ASI Series C196, Dordrecht, Reidel, Boston, 666 pp
Philpott AR, Carroll C, Hill JM (1996) Crystal-mush compaction and the origin of pegmatiticsegregation sheets in a thick floodbasalt flow in the Mesozoic Hartford Basin, Connecticut. J Petrol 37: 811–836
Puffer JH, Horter DL (1993) Origin of pegmatitic segregation veins within flood basalts. Geol Soc Am Bull 105: 738–748
Puffer JH, Volkert RA (2001) Pegmatoid and gabbroid layers in Jurassic Preakness and Hook Mountain basalts, Newark Basin, New Jersey. J Geol 109: 585–601
Raedeke LD, McCallum IS (1984) Investigations in the Stillwater Complex: Part II. Petrology and petrogenesis of the Ultramafic Series. J Petrol 25: 395–420
Richter RM, McKenzie DP (1984) Dynamical models for melt segregation from a deformable matrix. J Geol 92: 729–740
Samuelsson L (1973) Selective weathering of igneous rocks. Geol Surv Sweden C 690
Shirley DN (1986) Compaction of igneous cumulates. J Geol 94: 795–809
Sobral JM (1913) Contributions to the geology of the Nordingrå region. Diss. Univ. Upsala
Sonnenthal EL (1992) Geochemistry of dendritic anorthosites and associated pegmatites in the Skaergaard intrusion, East Greenland: evidence for metasomatism by a chlorine-rich fluid. J Volcanol Geoth Res 52: 209–230
Sparks RSJ, Huppert HE, Kerr RC, McKenzie DP, Tait SR (1985) Postcumulus processes in layered intrusions. Geol Mag 122: 555–568
Törnebohm AE (1877) Om Sveriges vigtigare diabas- och gabbroarter. Kongliga Svenska Vetenskapsakademins Handlingar, Vol. 14, No: 13
Wager LR, Brown GM (1968) Layered Igneous Rocks. Edinburgh, Oliver and Boyd, 558 pp
Wager LR, Brown GM, Wadsworth WJ (1960) Types of igneous cumulate. J Petrol 1: 73–85
Welin E, Lundqvist T (1975) K–Ar ages of Jotnian dolerites in Västernorrland County, central Sweden. Geologiska Föreningens i Stockholm Förhandlingar 97: 83–88